IL NUOVO CIMENTO **48 C** (2025) 39
DOI 10.1393/ncc/i2025-25039-8

COLLOQUIA: WPCF-Resonance 2023

Source function from two-particle correlations through deblurring: p-p and d $-$ α pairs

PIERRE NZABAHIMANA(1)(2), PAWEL DANIELEWICZ(1) and GIUSEPPE VERDE(3)

(1) *Facility of Rare Isotope Beams and Department of Physics and Astronomy, Michigan State University - East Lansing, MI 8824, USA*
(2) *Department of Physics, Albion College - 611 E. Porter St., Albion, MI 49224, USA*
(3) *Istituto Nazionale di Fisica Nucleare - Catania, Sicily, Italy*

received 23 July 2024

Summary. — In the study of heavy-ion collisions, two-particle correlation functions (CF) give insights into the space-time characteristics of nuclear systems. Typically, those characteristics are quantified with the so-called source function (SF) related to CF through the Koonin-Pratt (KP) convolution formula. Deducing SF from CF is, at the formal level, an imaging problem. Here, we use the Richardson-Lucy (RL) optical deblurring algorithm, employed elsewhere in imaging problems, to extract the SF from two-particle correlation function measurements. We apply the algorithm to the deuteron-alpha (d–α) and proton-proton (p-p) correlation data. In addition, we apply the Boltzmann-Uehling-Uhlenbeck (BUU) transport model to simulate the p-p source in heavy-ion collisions at low incident energies per nucleon (E/A). Comparing sources from BUU simulations with the RL algorithm results helps to understand the impact of fast and slow emissions on the sources. Consequently, we propose adding an analytically parametrized component to the BUU source to correct the missing secondary decay emissions in the model. In illustrating our approach, we rely on the p-p correlations measured in Ar + Sc reactions at E/A = 80 MeV.

1. – Introduction

Investigation of particle correlations in heavy-ion collision gives insights into the geometry and time development of the final stages of reactions [1-4], as well as phase-space distributions [5]. The final features get quantified with the relative distribution of particle pairs in the reaction, also known as source function (SF). The latter is here a focus, as a meeting point of the experiment and theory.

The correlation function is determined experimentally as the ratio of the probability of detecting two particles simultaneously to the product of probabilities of detecting single particles. Theoretically, it is approximated in terms of the so-called Koonin-Pratt (KP) formula, which expresses CF as a convolution of SF and the square of the relative wave function. It is necessary to understand relative wave functions within the studied particle pairs to connect SF in the reactions to the correlation functions (CF). These wave functions are obtained by solving the Schrödinger equation for the scattering problem with nuclear potentials obtained by fitting measured scattering phase shift (see, *e.g.*, ref. [6]). Often, SF is taken as a parameterized Gaussian function and fitted by comparing the KP formula to the measured correlation. Bias-free computation of the source function from a correlation function represents an imaging problem that, like elsewhere for imaging, invokes an inversion and thus may suffer from instabilities [7]. Here, rather than applying an inversion directly, we take inspiration from optical deblurring, which is an imaging problem, too. One successful strategy there that has already been used in nuclear physics to restore decay energy spectra measurements [8] and cope with detector inefficiencies and reaction-plane uncertainties [9] is the Richardson-Lucy (RL) algorithm [10, 11] that relies on the Bayes theorem and follows an iterative procedure to reach to a self-consistent solution. In a recent publication [12], we demonstrated by only using the correlation measurements and discretized transfer function, or kernel matrix (K), both positively defined as inputs, the RL algorithm can successfully restore a positive source function of a deuteron-alpha (d$-\alpha$) pair.

In this paper, we initiate our discussion by showcasing the application of the RL algorithm to restore the source function from d$-\alpha$ correlations measured in ^{40}Ar+^{27}Al reactions [13] (for additional details, readers are referred to ref. [12]). Next, we illustrate how the RL algorithm can be employed in parallel with the proton-proton (p-p) source function, computed using the Boltzmann-Uehling-Uhlenbeck (BUU) transport model, to better understand the p-p correlations. This analysis involves assessing the contribution of secondary decay emissions to the source function, which is absent in the BUU model's source (this subject will be discussed in detail in our upcoming paper) but is necessary to reproduce the measured p-p correlations. Here, the p-p correlations we use were measured in the Ar+Sc collision reaction at E/A=80 MeV [14].

The remainder of the paper is organized as follows: sect. 2 discusses the Koonin-Pratt formula; sect. 3 covers the deblurring method and its application in restoring the d$-\alpha$ source function. In sect. 4, we delve into the proton-proton source function from the BUU model and compare it to the p-p source function restored using the RL algorithm. Finally, we provide a summary in sect. 5.

2. – Two-particle correlations from Koonin-Pratt (PK) formula

Two-particle correlations are experimentally defined as the ratio of coincidence probability $P_2(\mathbf{p}_1, \mathbf{p}_2)$ and the product of single-particle probabilities $P_1(\mathbf{p}_{1,2})$: $C(\mathbf{q}) = P_2(\mathbf{p}_1, \mathbf{p}_2)/\big[P_1(\mathbf{p}_1)\, P_1(\mathbf{p}_2)\big]$, where $\mathbf{p}_1$ and $\mathbf{p}_2$ are particle momenta and $\mathbf{q} = \mu(\mathbf{p}_1 - \mathbf{p}_2)$ is the two-particle relative momentum. The correlation function is related to the source function S at relative separation $\mathbf{r} = \mathbf{r}_1 - \mathbf{r}_2$ at emission with the KP formula:

$$C(\mathbf{q}) = 4\pi \int_0^\infty dr\, r^2\, K(\mathbf{q}, \mathbf{r})\, S(\mathbf{r}) \equiv \int d^3r\, \overline{|\Psi^{(-)}_{\mathbf{q}}(\mathbf{r})|^2}\, S(\mathbf{r})\,. \tag{1}$$

Here, in the absence of spin, the kernel $K(\mathbf{q}, \mathbf{r})$ is equal to the square of the scattering wavefunction of particles 1 and 2, with outgoing boundary conditions. The normalization is such that the wavefunction squared averages to 1 over $\mathbf{r}$ at large distances. In the presence of spin, for a source independent of the spin directions, the kernel is equal to the wavefunction squared with spin indices summed over in the asymptotic region and averaged at the source location. It is common to use the wavefunction squared as a symbolic representation of the kernel, even in the case of spin. The kernel can be expanded in Legendre polynomials P_L [15]:

$$K(\mathbf{q},\mathbf{r}) = \frac{1}{2s+1}\sum_L (2L+1)A_L(\mathbf{q},\mathbf{r})P_L(\cos\theta)\,, \tag{2}$$

where θ is the angle between $\mathbf{q}$ and $\mathbf{r}$, $s=1$ is the deuteron spin, and

$$\begin{aligned} A_L(\mathbf{q},\mathbf{r}) = \sum_{l=0}^{l_{max}}\sum_{l'=0}^{l'_{max}}(2l+1)(2l'+1)\sum_{j=l-s}^{j=l+s}\sum_{j'=l'-s}^{j'=l'+s}(2j+1)(2j'+1) \\ \times \begin{pmatrix} l & l' & L \\ 0 & 0 & 0 \end{pmatrix}^2 \begin{Bmatrix} l & l' & L \\ j' & j & s \end{Bmatrix}^2 \mathrm{Re}\big[i^{l-l'}\,R^*_{j'l'}(q,r)\,R_{jl}(q,r)\big]\,. \end{aligned} \tag{3}$$

Here, $R_{j\ell}$ are radial wavefunctions, and the formula contains 3-j and 6-j symbols. When averaging CF over the angle of $\mathbf{q}$ relative to the emitting source, a relation between angle-averaged CF and angle-averaged SF emerges:

$$C(q) = 4\pi\int_0^\infty dr\, r^2\, K(q,r)\, S(r)\,, \tag{4}$$

where the isotropic kernel K stands for the r.h.s. of (2) with only the $L=0$ term after angle-averaging [6, 12].

The source function $S(\mathbf{r})$ on the r.h.s. of (1) or (4) is the probability distribution of particles 1 and 2 in their separation $\mathbf{r}$ in their center of mass, at the instant when they separate from the rest of the system and leave for the detectors. For a d-α pair, we obtain the radial wavefunctions in (3) and then the isotropic kernel K in (4) by solving Schrödinger equations with potentials taken from ref. [6].

The left panel of fig. 1 displays the contour plot of the isotropic kernel K for a d–α pair. Various features of the kernel can be seen there. The dip in kernel values at low q is tied to the Coulomb repulsion. The ridge near $r \sim 7\,\mathrm{fm}$ is tied to nuclear attraction. The peaks for $q \simeq 42$ and $84\,\mathrm{MeV}/c$ correspond to the resonances in the $^3\mathrm{D}_3$ state and in the $^2\mathrm{D}_1$ and $^2\mathrm{D}_2$ states, respectively, with the peaks overlapping for the last two (see ref. [6] for more details about interactions in these channels). The right panel shows d$-\alpha$ correlations, obtained using the KP formula (4) with a Gaussian source characterized by an exemplary radius $R_0 = 5$ fm. The peaks around 42 and $84\,\mathrm{MeV}/c$ reflect the structures observed in K and attributed to the resonance states in ^{6}Li at the energies of $E = 2.18$, 4.31, and 5.6 MeV.

3. – Deblurring

When progressing from the side of correlation data to infer emission sources, we employ optical deblurring [8, 9, 16] and now introduce the basics of that approach. The blurring relation between a measured distribution g and a sought physical distribution $\mathcal{G}$, inaccessible directly due to a blurring, can be generally stated as

$$g(t') = \int dt\, B(t',t)\, \mathcal{G}(t)\,. \tag{5}$$

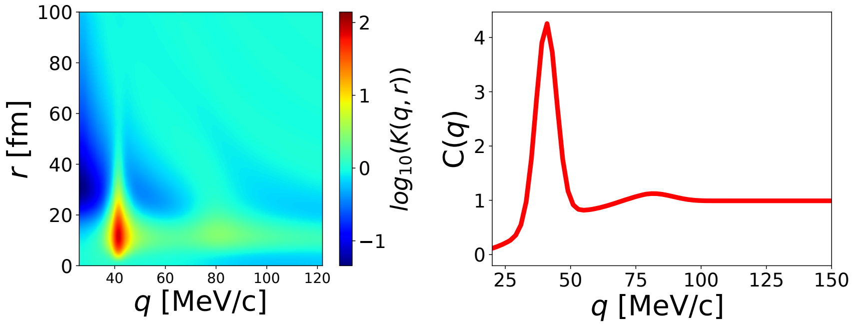

Fig. 1. – d–α correlation in theoretical perspective. The left panel displays a logarithmic contour plot in q–r for the isotropic kernel $K(q,r)$ in the KP relation. The right panel displays the $d-\alpha$ correlation function, obtained using the KP formula (4) with a Gaussian source.

Here, t' is the argument in the measurement domain, t is the argument of the sought distribution, and $B(t',t)$ is the blurring or response function describing how g responds to a change in $\mathcal{G}$. The task is to assess the function $\mathcal{G}$. We achieve this following the RL algorithm discussed next.

Under domain discretization, the relation in (5) takes the form of a matrix relation between two vectors:

$$g_i = \sum_i B_{ij}\, \mathcal{G}_j \,. \tag{6}$$

A deblurring method, such as RL, seeks to determine the function $\mathcal{G}$ when knowing g and B. To arrive at the RL strategy, a backward relation between g and $\mathcal{G}$ is invoked, which involves a response function D that is complementary to B [6]. Requiring fulfillment of a Bayesian-form relation involving B and D, leads to iterations for $\mathcal{G}$:

$$\mathcal{G}_j^{(\mathfrak{n}+1)} = \mathcal{G}_j^{(\mathfrak{n})} \frac{\sum_i B_{ji}\, w_i\, \frac{g_i}{g_i^{(\mathfrak{n})}}}{\sum_k B_{jk}\, w_k} \equiv \mathcal{G}_j^{(\mathfrak{n})}\, A_j^{(\mathfrak{n})} \,. \tag{7}$$

Here, $\mathfrak{n}$ is the iteration index, $A^{(\mathfrak{n})}$ is an amplification factor, and $g_i^{(\mathfrak{n})} = \sum_j B_{ij}\, \mathcal{G}_j^{(\mathfrak{n})}$ is prediction for the measurement at $\mathfrak{n}$'th iteration. The weights w in (7) can focus attention on the region of relative momenta in the correlation function that is dominated by interactions within the particle pair, which is believed to test the source particularly well. Typically, the iterations, indexed by $\mathfrak{n}$ in eq. (7), stop when the ratio $g_i/g_i^{(\mathfrak{n})}$ approaches unity.

While the deblurring algorithms have been introduced for processing of optical images, there is an obvious analogy in the mathematical structure of the optical problem and one in the source inference, with the mapping: $g \leftrightarrow C$, $B \leftrightarrow K$, and $\mathcal{G} \leftrightarrow S$. The success of optical deblurring algorithms is largely due to all three quantities in the blurring relation being positive definite, and this is the case with the KP formula.

The data that we use to infer the source function are the d-α correlations measured at forward angles $0.7^\circ < \theta < 7^\circ$ in $44\,\mathrm{MeV/nucl}$ $^{40}\mathrm{Ar}+^{27}\mathrm{Al}$ collisions by Ghetti *et al.* [13], displayed in fig. 2(a) as points. The narrow peak in the measurements around

$q \sim 40\,\mathrm{MeV}/c$ and a hint of a broad peak around $q \sim 84\,\mathrm{MeV}/c$ underscore the complementary utility of correlations in identifying resonances and other aspects of interactions. That utility is particularly important when dealing with short-lived reaction products [17]. The source function obtained by feeding the data from panel (a) into eq. (4) and applying the RL algoritm is represented as a solid line in the panel (b). The shaded regions in panel (b) represent the range of results obtained when resampling the input data to (4) consistently with errors, cf. [8, 12]. The solid line and shaded regions in (a) show results when the forward relation (4) is applied to the sources inferred under data resampling. The relatively smaller size of errors in (a) for different q than for r in (b) stems from the fact that the results in (b) come out correlated between different r. For comparison, we show also a Gaussian source with a radius $R_0 = 4.5\,\mathrm{fm}$. Notably, the Gaussian source is normalized to integrate to $\lambda = 0.49$, missing probability, while the RL sources integrate to 1. The two types of sources differ in the tails that are not exposed in panel (b).

4. – $p-p$ correlations: Transport model and deblurring

When a transport model describes the production of particular particle species, a source may be directly constructed there. The Boltzmann-Uhlenbeck-Uehling (BUU) simulation codes, utilized for intermediate-energy heavy-ion collisions, follow the evolution of semiclassical single-nucleon phase-space distributions $f = f(\mathbf{p}, \mathbf{r}, t)$ by solving

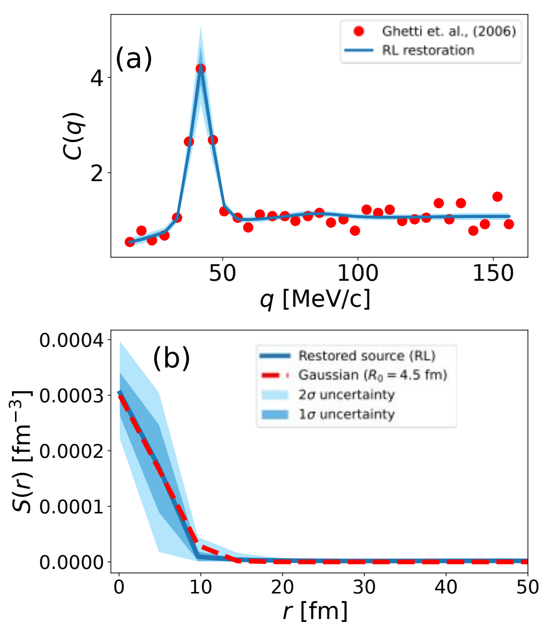

Fig. 2. – (a) Deuteron-alpha correlation *vs.* relative-momentum magnitude q. Data from Ghetti *et al.* measurements [13] from the $E/A = 44\,\mathrm{MeV}$ $^{40}\mathrm{Ar}+^{27}\mathrm{Al}$ reaction are represented by points. Line and shaded regions display results behind the RL source restoration. (b) The solid line with the shaded areas represents the source from RL deblurring of the data in panel (a). For comparison, the dashed line represents a Gaussian source function with radius $R_0 = 4.5\,\mathrm{fm}$ [12], multiplied by $\lambda = 0.49$.

coupled one-body transport equations [18, 19],

$$\left(\frac{\partial}{\partial t} + \nabla_{\mathbf{p}}\varepsilon \cdot \nabla_{\mathbf{r}} - \nabla_{\mathbf{r}}\varepsilon \cdot \nabla_{\mathbf{p}}\right) f = I_{col}(\sigma_{in}, \{f\})\,. \tag{8}$$

With $\varepsilon = p^2/2m + U(\mathbf{r}, \mathbf{p})$, the left-hand side of eq. (8) is the one-body Liouville equation in the presence of a self-consistent mean-field U. On the right-hand side, I_{col} is the collision integral that accounts for changes in f due to nucleon-nucleon collisions [18, 19].

The two-particle source function can be estimated from a BUU simulation following the formula:

$$S^{BUU}(r) = \frac{\int d^3R\, f(\mathbf{P}/2, \mathbf{R} + \mathbf{r}/2, t')\, f(\mathbf{P}/2, \mathbf{R} - \mathbf{r}/2, t')}{\left[\int d^3r\, f(\mathbf{P}/2, \mathbf{R}, t')\right]^2}\,. \tag{9}$$

Here, $\mathbf{r}$ is the relative position within the particle pair, $\mathbf{R} = (\mathbf{r}_1 + \mathbf{r}_2)/2$ is the center of mass coordinate and $\mathbf{P}$ is the total momentum of the particles at the time when the last particle is emitted, see [14] and references within. The phase-space distribution of particles with momentum $\mathbf{P}/2$, position $\mathbf{r}_{1,2}$, and at time t' after both particles have been emitted is described by a Wigner distribution $f(\mathbf{P}/2, \mathbf{r}_{1,2}, t')$ [14]. For practical calculational purposes, the record for the late-time Wigner functions is taken at the emission into vacuum, with the Wigner functions read off from the final emission functions g with $f(\mathbf{P}/\mathbf{2}, \mathbf{r}, t') = \int_{-\infty}^{t'} dt\; g(\mathbf{P}/2, \mathbf{r} - \mathbf{P}(t'-t)/2m, t)$. The interplay of locations and time evolution in arriving at the relative source shows how that source S tests the space-time characteristics of the final stages of the reactions.

To obtain a p-p correlation function from a transport model, we simply replace $S(r)$ in eq. (4) by $S^{BUU}(r)$ of eq. (9). With an intention to confront the transport model [18] with data [14], we simulate a central ^{36}Ar $+^{45}$ Sc collision at 80 AMeV. In comparing to data it is usually of interest whether the comparison may provide access to the nuclear Equation Of State (EOS). We test the sensitivity of S^{BUU} to EOS in fig. 3 but find it weak for the angle-averaged source in the momentum bracket considered for the system [14].

Two types of emissions are expected during a heavy ion collision: early, fast, largely non-equilibrium emission and late sequential-decay emission [20]. Fast contributions to the source largely reflect geometry, specifically the spatial extent over which particles

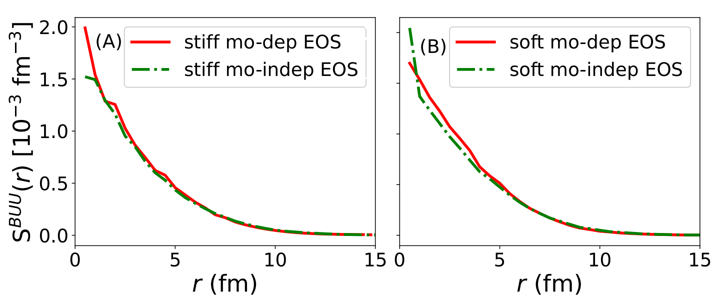

Fig. 3. – Two-proton source function from BUU simulation of the ^{36}Ar $+^{45}$ Sc collision at 80 MeV/nucleon and $b = 1.9$ fm, in the 200-400 MeV/c range of total momentum. The two panels display results for stiff (a) and soft (b) EOS with and without momentum-dependence. We do not find much dependence on EOS in the angle-averaged sources in the particular system.

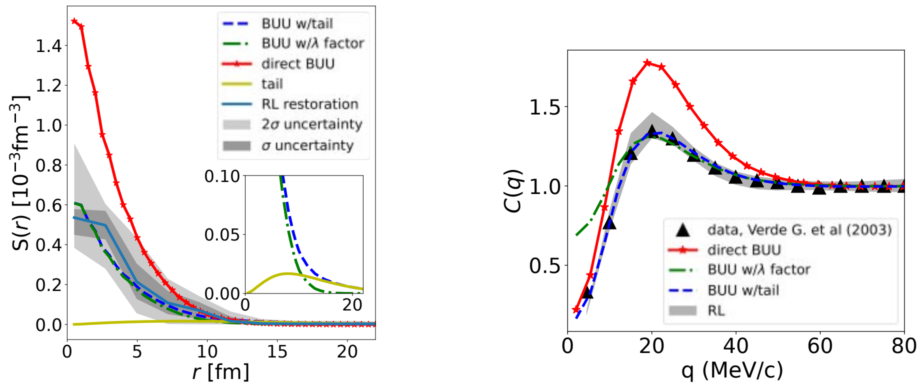

(a) (b)

Fig. 4. – Source (a) and correlation (b) for proton pairs at total momentum 200-400 MeV/c in central ^{36}Ar $+^{45}$ Sc collisions at 80 MeV/nucleon. The triangles in (b) represent the correlation data from ref. [14]. The shaded regions in (a), with a central line, represent the results from deblurring the data in (b). The corresponding correlation results are indicated in (a). Finally, BUU results are depicted in both panels in a direct form, with λ multiplication and tail addition. For extra insight, the tail alone is represented in panel (a) and the inset there shows details in the fall-off of the theoretical distributions.

with similar velocity may be found, limited by variation in collective velocity. On the other hand, late contributions reflect the spread of times over which decays take place, including possible multifragmentation. Fast emission contributes to the low-r region of S while long-term emission contributes to high-r features. Notably, a BUU transport model cannot describe the long-term emission and, thus, the high-r contributions to S. In fig. 3, the sources indeed lack long-r tails, *i.e.*, rapidly approaching 0 with an increase in r, see also ref. [14].

In the current literature, researchers have attempted to correct the p-p correlation function obtained from BUU simulations by multiplying the BUU source with a factor λ, see refs. [6, 14, 20], similarly to the case of the Gaussian source in fig. 2. The underlying presumption is that the faction $(1-\lambda)$ of the experimental p-p pairs contains at least one nucleon from the slow processes not there in the transport model. The correct behavior of the correlation function at high q is recovered by constructing the correlation function for the comparison to data as $C = \lambda\, C^{BUU} + (1-\lambda)$, where C^{BUU} is obtained with the source before reduction.

Here, we propose to augment the procedure in confronting the transport prediction to data by supplementing the transport source with an exponential representing the secondary-decay contributions:

$$S(r) = \lambda\, S^{BUU}(r) + \frac{1-\lambda}{96\pi B^5}\, r^2\, \exp(-r/B)\,, \tag{10}$$

where λ and B are adjustable parameters. The idea is to capture the fraction $(1-\lambda)$ of pairs to which the late emission contributes and the characteristic source fall-off associated with that contribution.

The transport model with and without the late-state emission addition, correlation data, and deblurring for central ^{36}Ar $+^{45}$ Sc collisions at 80 MeV/nucleon are confronted with each other in fig. 4. The data [14] for p-p pairs from the total momentum range

200-400 MeV/c are represented with triangles in panel (b). Source results from the RL deblurring of the data are shown in panel (a), and the corresponding correlation results are shown in (b). Finally, transport results are represented in both panels. Since there is little difference between the sources for soft and stiff EOSs, we chose the stiff momentum-independent EOS as an example. We show three variants of transport results for a source directly taken from the BUU calculation, a source reduced by λ, and an added long-emission tail. We use $\lambda = 0.4$ and $B = 4$ fm in eq. (10).

Using the λ reduction alone, as typical for the literature, we obtain consistency between the RL restored source and BUU up to $r \sim 10$ fm, but not above, and consistency between the theoretical correlation function and data from 14 MeV/c on. We get consistency at higher r and lower q with tail addition. The grasp of physics is much better with the tail, even though we do not particularly optimize those added parameters.

5. – Summary

We discussed using the RL algorithm to infer the source functions for d–α and p–p pairs from correlations measured in Ar+Al at 44 MeV/nucl and Ar+Sc at 80 MeV/nucl collisions, respectively. The inferred sources exhibit tails at large separations between the particles that can be attributed to longer-term emissions from the systems. When carrying BUU transport calculations of proton emission, we find a relatively compact source for proton pairs. However, we find that we can get a reasonable consistency between the calculated source and correlation function if we supplement the BUU source with a phenomenological tail representing contributions to the source from long-term emissions absent from BUU. For more details about application of the RL algorithm to correlations, we refer the readers to refs. [8, 9, 12].

* * *

This work was supported by the U.S. Department of Energy Office of Science under Grant No. DE-SC0019209.

REFERENCES

[1] Bauer W., *Prog. Part. Nucl. Phys.*, **30** (1993) 45.
[2] Heinz U., Tomášik B., Wiedemann U. A. and Wu Y. F., *Phys. Lett. B*, **382** (1996) 181.
[3] Koonin S. E., *Phys. Lett. B*, **70** (1977) 43.
[4] Pratt S., *Phys. Rev. Lett.*, **53** (1984) 1219.
[5] Bertsch G. F., *Phys. Rev. Lett.*, **72** (1994) 2349; **77** (1996) 789(E).
[6] Nzabahimana P., *Particle correlations in heavy-ion collisions*, PhD Thesis, Michigan State University (2023).
[7] Brown D. A. and Danielewicz P., *Phys. Lett. B*, **398** (1997) 252.
[8] Nzabahimana P., Redpath T., Baumann T., Danielewicz P., Giuliani P. and Guèye P., *Phys. Rev. C*, **107** (2023) 064315.
[9] Danielewicz P. and Kurata-Nishimura M., *Phys. Rev. C*, **105** (2022) 034608.
[10] Richardson W. H., *J. Opt. Soc. Am.*, **62** (1972) 55.
[11] Lucy L. B., *Astron. J.*, **79** (1974) 745.
[12] Nzabahimana P. and Danielewicz P., *Phys. Lett. B*, **846** (2023) 138247.
[13] Ghetti R., Helgesson J., Lanzanò G., De Filippo E., Geraci M., Aiello S., Cavallaro S., Pagano A., Politi G., Charvet J., Dayras R., Pollacco E., Volant C., Beck C., Mahboub D. and Nouicer R., *Nucl. Phys. A*, **765** (2006) 307.

[14] Verde G., Danielewicz P., Brown D. A., Lynch W. G., Gelbke C. K. and Tsang M. B., *Phys. Rev. C*, **67** (2003) 034606.
[15] Danielewicz P., Singh P. and Lee J., *Nucl. Phys. A*, **958** (2017) 147.
[16] Zech G., *Nucl. Instrum. Methods Phys. Res. Sect. A*, **716** (2013) 1.
[17] Grenier F., Chbihi A., Roy R., Verde G., Thériault D., Frankland J., Wieleczko J., Borderie B., Bougault R., Dayras R., Galichet E., Guinet D., Lautesse P., Le Neindre N., Lopez O., Moisan J., Nalpas L., Napolitani P., Pârlog M., Rivet M., Rosato E., Tamain B., Vient E. and Vigilante M., *Nucl. Phys. A*, **811** (2008) 233.
[18] Danielewicz P., *Nucl. Phys. A*, **673** (2000) 375.
[19] Wolter H., Colonna M., Cozma D., Danielewicz P., Ko C. M., Kumar R., Ono A., Tsang M. B., Xu J., Zhang Y.-X., Bratkovskaya E., Feng Z.-Q., Gaitanos T., Le Fèvre A., Ikeno N., Kim Y., Mallik S., Napolitani P., Oliinychenko D., Ogawa T., Papa M., Su J., Wang R., Wang Y.-J., Weil J., Zhang F.-S., Zhang G.-Q., Zhang Z., Aichelin J., Cassing W., Chen L.-W., Cheng H.-G., Elfner H., Gallmeister K., Hartnack C., Hashimoto S., Jeon S., Kim K., Kim M., Li B.-A., Lee C.-H., Li Q.-F., Li Z.-X., Mosel U., Nara Y., Niita K., Ohnishi A., Sato T., Song T., Sorensen A., Wang N. and Xie W.-J., *Prog. Part. Nucl. Phys.*, **125** (2022) 103962.
[20] Verde G., Brown D. A., Danielewicz P., Gelbke C. K., Lynch W. G. and Tsang M. B., *Phys. Rev. C*, **65** (2002) 054609.